AIP | Review of Scientific Instruments

A photoelastic-modulator-based motional Stark effect polarimeter for ITER that is insensitive to polarized broadband background reflections

A. Thorman, C. Michael, M. De Bock, and J. Howard

Citation: Review of Scientific Instruments **87**, 073504 (2016); doi: 10.1063/1.4958648
View online: http://dx.doi.org/10.1063/1.4958648
View Table of Contents: http://scitation.aip.org/content/aip/journal/rsi/87/7?ver=pdfcov
Published by the AIP Publishing

A photoelastic-modulator-based motional Stark effect polarimeter for ITER that is insensitive to polarized broadband background reflections

A. Thorman,[1,a)] C. Michael,[1] M. De Bock,[2] and J. Howard[1]
[1]*Plasma Research Laboratory, Research School of Physics and Engineering, Australian National University, Canberra, ACT 0200, Australia*
[2]*ITER Organization, Route de Vinon-sur-Verdon, 13067 St Paul-lez-Durance, France*

(Received 21 December 2015; accepted 29 June 2016; published online 20 July 2016)

A motional Stark effect polarimeter insensitive to polarized broadband light is proposed. Partially polarized background light is anticipated to be a significant source of systematic error for the ITER polarimeter. The proposed polarimeter is based on the standard dual photoelastic modulator approach, but with the introduction of a birefringent delay plate, it generates a sinusoidal spectral filter instead of the usual narrowband filter. The period of the filter is chosen to match the spacing of the orthogonally polarized Stark effect components, thereby increasing the effective signal level, but resulting in the destructive interference of the broadband polarized light. The theoretical response of the system to an ITER like spectrum is calculated and the broadband polarization tolerance is verified experimentally. *Published by AIP Publishing.* [http://dx.doi.org/10.1063/1.4958648]

I. INTRODUCTION

The transport and stability properties of magnetic confinement fusion devices are intrinsically coupled to the internal magnetic field distribution. Motional Stark effect (MSE) polarimetry is a widely used diagnostic tool for estimating the toroidal current profile in tokamaks.[1,2] The technique is also capable of determining the efficiency of radio frequency heating from measurements of the plasma diamagnetism[3] as well as measuring non-inductive driven currents based on gradients in the magnetic field profile.[4–6]

MSE diagnostics observe the Doppler shifted Balmer-alpha emission from a high energy neutral beam injected into the plasma. A strong motional electric field in the rest frame of the beam atoms causes the emission to be split, by the linear Stark effect, into orthogonally polarized π and σ components.[7] Provided the plasma radial electric field is small, a polarimetric measurement of the beam emission will reveal the orientation of the magnetic field component perpendicular to the neutral beam velocity.[8]

For the multichannel MSE polarimetry system planned for ITER, it is anticipated that a significant source of systematic error will be the contribution of partially polarized broadband reflections from the metallic walls and surfaces. These reflections have been observed to produce systematic errors on Alcator C-Mod,[9] JT-60U[10] and Tore-Supra[11] where deviations in the MSE angle of up to 2° are seen during radio frequency heating. Reflected Bremsstrahlung, the main source of the partially polarized light, is expected to be more significant on ITER due to the increased plasma density and volume, while the beam signal is also expected to be relatively weaker due to the greater beam attenuation.[12]

A number of strategies have been devised to compensate for this broadband component. For example, emission at a nearby wavelength that is free of atomic emission can be subtracted from the MSE signal as implemented on JT-60U.[10] A more comprehensive polychromator system has been implemented on Alcator C-Mod to analyse the σ and both π components as well as monitoring nearby red and blue shifted backgrounds.[9] Spectrometer based static polarimetry is also amenable to broadband background subtraction.[13] Another option is to model the partially polarized emission based on accurate knowledge of the wall's reflective properties and the plasma conditions, but the accuracy of such a calculation is unproven for ITER-like conditions. A system that is intrinsically tolerant to background reflections is desirable.

The most widely used MSE polarimetry method[1,14] and the one envisaged for ITER utilises two photoelastic modulators (PEMs) to modulate the polarization state of the light before a polarizer converts this to an intensity modulation. For each observation position, a narrowband tuned filter transmits a portion of the MSE multiplet spectrum with a high polarization (π or σ) fraction for analysis. The polarization angle is encoded in the amplitude of the second harmonics of the PEM frequencies. Second harmonic detection has been preferred for high precision broadband polarimetry due to surface-dichroism affecting first harmonic detection.[15]

An alternative to PEM-based MSE polarimetry has been proposed recently.[16,17,21] Imaging motional Stark effect (IMSE) observes light from the full multiplet, achieving spectral discrimination and high net polarization fraction with a birefringent sinusoidal interference filter. This approach is amenable to two dimensional imaging of the beam emission as there is no need to precisely track the beam Doppler shift. It allows greater spectral throughput, avoids the need to tune individual filters and, of particular relevance to ITER, is also tolerant of broadband polarized background contamination.[16,18]

In this paper we introduce an alternative PEM-based polarimetry system tolerant to broadband polarized background that combines techniques from the standard PEM

a)Electronic mail: alexander.thorman@anu.edu.au

approach and the IMSE approach. In Section II we describe the standard dual PEM technique along with a single PEM system capable of measuring the polarization angle. The principles of IMSE are reviewed in Section III and adapted to PEM based systems. Bench-top experimental results are presented and the polarimeter response is assessed for a model ITER spectrum in Sections IV and V respectively.

II. MSE POLARIMETRY

The general state of partially polarized light can be described by the Stokes vector

$$\begin{aligned} \boldsymbol{s} &= (s_0, s_1, s_2, s_3) \\ &= I\,(1,\, p\cos 2\epsilon \cos 2\theta,\, p\cos 2\epsilon \sin 2\theta,\, p\sin 2\epsilon)\,, \end{aligned} \quad (1)$$

where I is the radiant flux, p is the degree of polarization, θ is the orientation of the major-axis of the polarization ellipse, and ϵ is the ellipticity angle.

The Balmer-alpha Stark multiplet results from 36 transitions (when electron spin is neglected) of 15 different energies. There are nine symmetrically spaced lines with significant transition probability, and three produce a central σ cluster polarized perpendicular to the motional electric field, while two groups of three produce the π wings polarized parallel to the field. For our purposes, the spectrum can be approximated by three peaks whose Stokes vectors are given by

$$\begin{aligned} \boldsymbol{s_\sigma} &= \frac{I_0(1+\cos^2\psi)}{2}(1,\, p_\sigma \cos 2\theta_\sigma,\, p_\sigma \sin 2\theta_\sigma,\, 0), \\ \boldsymbol{s_{\pi\pm}} &= \frac{I_0 \sin^2\psi}{4}(1,\, -\cos 2\theta_\sigma,\, -\sin 2\theta_\sigma,\, 0), \end{aligned} \quad (2)$$

where ψ is the angle between the line of sight and the motional electric field, $p_\sigma = \sin^2\psi/(1+\cos^2\psi)$, and θ_σ is the angle of the σ polarization relative to some chosen axes. Each of the three components has a spectral line shape with central angular frequencies given by $\omega_\sigma = \omega_0$ and $\omega_{\pi\pm} = \omega_0 \pm \Delta\omega$ where ω_0 is the Doppler shifted centre angular frequency, $\Delta\omega = 3\Delta E/\hbar$ is the angular frequency separation between the central π and σ components, ΔE is the energy splitting between Stark transitions, and $\hbar$ is the reduced Plank constant. Taking the spectral broadening into account, the MSE spectrum can be simplified to

$$\boldsymbol{s}(\omega) = I(\omega)(1,\, p(\omega)\cos 2\theta_\sigma,\, p(\omega)\sin 2\theta_\sigma,\, 0), \quad (3)$$

where $-1 \le p(\omega) \le 1$ and $p(\omega) \approx -1$ in parts of the spectrum with a majority of π light and $p(\omega) \approx p_\sigma$ in regions with a majority of σ light. This simplified spectrum neglects Stark-Zeeman coupling which slightly elliptizes the transitions. Integrated over the MSE spectrum the light has no net polarization when the upper states of the transition have equal populations, so some spectral discrimination is needed to obtain θ_σ.

Broadband background radiation reflected off a surface with different s and p reflectivities will give rise to partially polarized light that can represented by

$$\boldsymbol{s}_b = I_b\,(1, p_b\cos 2\epsilon_b \cos 2\theta_b, p_b \cos 2\epsilon_b \sin 2\theta_b, p_b \sin 2\epsilon_b)\,. \quad (4)$$

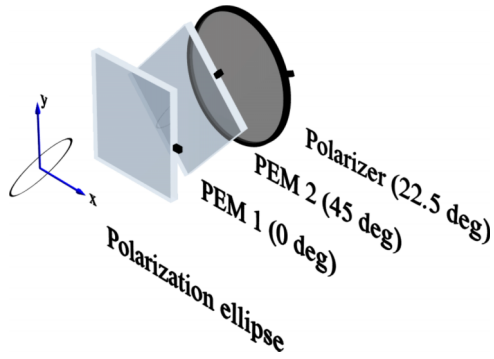

FIG. 1. Schematic model of standard double PEM arrangement for MSE polarimetry.

This light will add to the beam emission distorting the observed polarization orientation.

A. Standard dual PEM polarimetry

Figure 1 shows a schematic layout of the conventional double PEM polarimeter. The first PEM is oriented horizontally and modulates s_2 at even harmonics ω_1. The second PEM oriented diagonally, then modulates s_1 at even harmonics of ω_2. The phase modulated waves are combined interferometrically by a polarizer oriented at 22.5° to produce the overall signal,

$$\begin{aligned} 2\sqrt{2}S = \sqrt{2}s_0 &+ s_1\cos\delta_2 + s_2(\cos\delta_1 + \sin\delta_1 \sin\delta_2) \\ &+ s_3(\sin\delta_1 - \cos\delta_1 \sin\delta_2)\,, \end{aligned} \quad (5)$$

where $\delta_n = \phi_n \sin\omega_n t$ is the modulated phase shift imposed by the PEMs. The modulation amplitudes at the second harmonic of ω_1 and ω_2 are given by

$$S_{2\omega_1} = (A\sin 2\theta_\sigma + B\sin 2\theta_b)\,J_2(\phi_1), \quad (6)$$

$$S_{2\omega_2} = (A\cos 2\theta_\sigma + B\cos 2\theta_b)\,J_2(\phi_2), \quad (7)$$

where $A = (p_\sigma I_\sigma - I_\pi)/\sqrt{2}$; $B = p_b \cos 2\epsilon_b I_b/\sqrt{2}$; I_σ, I_π, and I_b are the radiant fluxes of the σ, π, and background emission passing through the filter. When $A \gg B$ the ratio of these amplitudes gives an expression for θ_σ as the modulation depths ϕ_n are known and can be verified from the ratio of the second and fourth harmonic amplitudes. To maximise the signal a narrowband filter selects a region in the Doppler shifted spectrum that is dominated by π or σ emission. A multi-channel measurement therefore requires a set of discrete narrowband filters tuned for each viewing position at fixed beam energy.

B. Phase single PEM polarimetry

Instead of using separate PEMs to individually modulate s_1 and s_2, it is possible to use a single PEM to modulate both as illustrated in Fig. 2. An initial quarter-wave plate at 0° will interchange s_2 and s_3 such that the PEM oriented at 45° modulates both s_1 and s_2. The s_2 component is now encoded at the odd harmonics of the oscillation frequency.

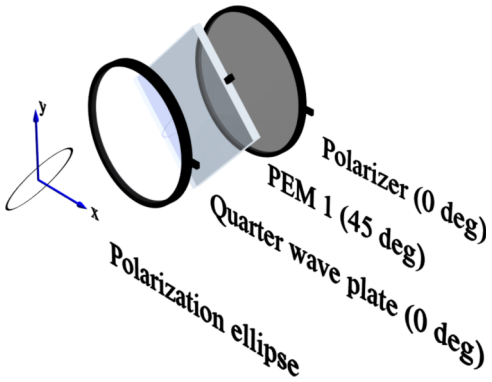

FIG. 2. Schematic model of the modified single PEM arrangement for MSE polarimetry.

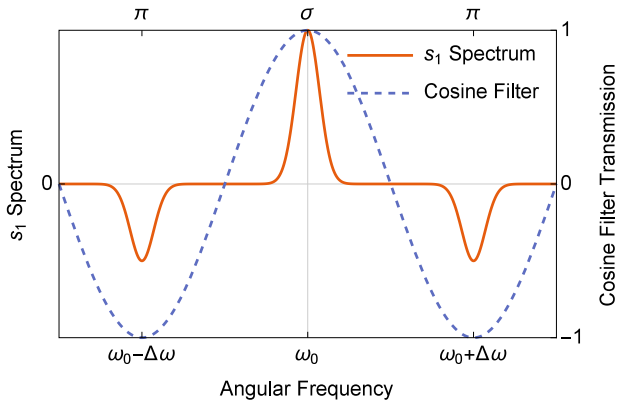

FIG. 3. Simplified spectrum of the MSE multiplet (solid line) and an ideal cosine filter (dashed line). To achieve the maximum signal, the cosine filter half-period must match the spacing between the central π and σ components and its phase must be modulated to ensure it periodically aligns with the spectrum for all possible Doppler shifts.

The generalised signal produced by this system is given by

$$\frac{2S}{I} = 1 + p\cos 2\epsilon \cos(2\theta - \delta_1) \tag{8}$$

and the modulation amplitudes at $n\omega_1$ ($n > 0$) are given by

$$S_{n\omega_1} = \begin{cases} s_1 J_n(\phi_1) & n \text{ even} \\ s_2 J_n(\phi_1) & n \text{ odd} \end{cases}. \tag{9}$$

With only a single PEM the frequency spectrum does not contain cross harmonics, leading to a greater available bandwidth. Additionally the signal is stronger than the dual PEM signal by a factor of $\sqrt{2}$. However the system cannot measure the ellipticity angle unlike the dual PEM system which carries the s_3 information at the first harmonic of ω_1.

III. COHERENCE BASED MSE

A. Net polarization fraction principle

Without spectral discrimination the net polarization fraction is zero when integrating over the entire MSE spectrum. Instead of transmitting only a portion of the MSE multiplet with high polarization fraction, the coherence based technique applies a sinusoidal filter over the full multiplet to achieve a large net polarization fraction. In this subsection the principle for achieving a large net polarization fraction is outlined, while the background suppression and modulation strategies are described in Subsections III B–III E.

Consider an optical system with a birefringent waveplate with diagonally oriented axes followed by a horizontal polarizer. For light initially polarized horizontally the waveplate will produce a phase delay, ϕ, between the fast and slow rays such that the light interferes when recombined at the polarizer. For a general input, the signal would be

$$2S = \int_0^\infty s_0(\omega) + s_1(\omega)\cos\phi(\omega) - s_3(\omega)\sin\phi(\omega)d\omega, \tag{10}$$

where ω is the optical angular frequency.

When considering the MSE signal, we aim to select a delay such that the filter, $\cos\phi(\omega)$, overlaps with $s_1(\omega)$ as illustrated in Fig. 3. A wide (≈10 nm) interference filter transmits the full energy MSE multiplet and restricts other coherent polarization sources such as unshifted Balmer-alpha, half and third energy beam components, and impurity emissions. For frequencies ω near ω_0, a birefringent crystal of thickness L and birefringence $B(\omega)$ will produce a phase difference between fast and slow axes of

$$\phi = \frac{\omega L B(\omega)}{c} \approx \phi_0 + \phi_0\kappa\frac{\omega - \omega_0}{\omega_0}, \tag{11}$$

where

$$\phi_0 = \frac{\omega_0 L B(\omega_0)}{c}, \tag{12}$$

$$\kappa = 1 + \frac{\omega_0}{B(\omega_0)}\frac{dB}{d\omega}\Big|_{\omega=\omega_0}. \tag{13}$$

To obtain a filter period like that in Fig. 3, we select a birefringent crystal of thickness L_0 such that the filter half-period matches the spacing, $\Delta\omega$, between the orthogonally polarized π and σ components,

$$\phi_0\kappa\Delta\omega/\omega_0 = \pi \tag{14}$$

leading to

$$L_0 = \frac{\pi c}{\Delta\omega\kappa B(\omega_0)}. \tag{15}$$

When considering a realistic MSE multiplet spectrum, the optimal crystal thickness will be closer to $0.8L_0$ as plotted in the right hand axes of Fig. 4. For a sinusoidal filter the maximum polarization throughput is not sensitively dependent on the crystal thickness as illustrated in Fig. 5. With a PEM modulating the delay of the waveplate, the system is tolerant to large changes in the beam velocity and suffices to view the full range of Doppler shifts across the field of view of the beam.

Strategies to encode the polarization orientation and modulate the sinusoidal filter phase ϕ_0 to periodically achieve the maximum signal are discussed in Section III C and III D. A strategy to continually achieve the maximum signal is described in Section III E.

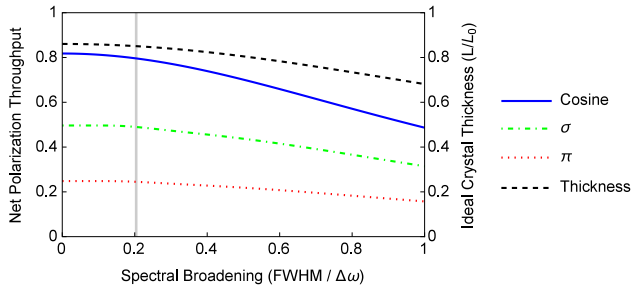

FIG. 4. Throughput of optimised cosine (solid line), σ top-hat narrowband (dotted-dashed line), and π top-hat narrowband (dotted line) filters as a function of Gaussian spectral broadening. The crystal thickness required for the optimal cosine filter is plotted with the dashed line. The vertical gridline indicates the broadening relevant to the ITER diagnostic beam described in Section V. This assumes only the linear Stark effect and statistical upper state populations.

B. Inherent suppression of broadband polarized background

The use of a sinusoidal filter has the advantage that broad background signals will destructively interfere. With a realistic spectrum for the $s_1(\xi)$ component and an interference filter profile of $f(\xi)$, where $\xi = (\omega - \omega_0)/\omega_0$, the net contribution of the $\cos(\phi)$ term (see Eq. (10)) will be related to the Fourier transform

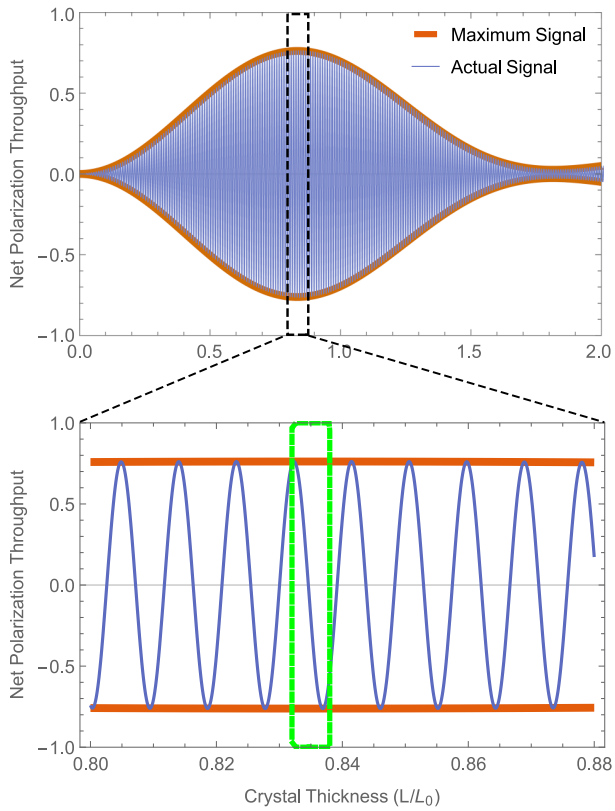

FIG. 5. Signal through the cosine filter as a function of crystal thickness for a realistic MSE spectrum. Modulation over $\approx\pi$ rad (green boxed region) ensures that the maximum signal is reached. This is similar to an IMSE system where $\approx$100 waves are used to spatially modulate the image. A wide cosine filter ($L \ll L_0$) will have weak signal as the total multiplet is unpolarized. The optimal crystal thickness here is 83% of the back of envelope calculation in Eq. (15).

$$\int_{-\infty}^{\infty} s_1(\xi) f(\xi) \cos\phi(\xi) d\xi \approx |(\hat{s_1} * \hat{f})(\phi_0\kappa)| \cos(\phi_0), \tag{16}$$

where $\hat{}$ denotes the Fourier transform and $*$ the convolution.

For broadband partially polarized background, we approximate that $I_b(\xi) = I_b$ is constant and select a filter with centre angular frequency ω_b such that ϕ_b is defined similarly to Equation (12). In this case the net contribution from the partially polarized background is

$$p_b I_b |\hat{f}(\phi_b\kappa)| \cos\phi_b. \tag{17}$$

We can completely suppress the background by selecting a filter that apodizes the sinusoidal filter with equal intensity in the positive and negative half-periods of the sinusoidal filter. This is achieved when we select an interference filter width such that $\hat{f}(\phi_b\kappa) = 0$. For example, in the case of a top-hat filter, the width required would apodize an integer number of periods of the cosine filter or mathematically,

$$\omega_{FW} = \frac{2\pi m\omega_b}{\phi_b\kappa} = \frac{2\pi mc}{LB(\omega_b)\kappa}. \tag{18}$$

Alternatively with a smooth Lorentzian interference filter profile, the polarized background signal is suppressed exponentially as the filter full width at half-maximum (FWHM) is increased. With a single filter of correct width, it is possible to view all channels and achieve any required level of background suppression.

Additionally the filter centre angular frequency ω_b could be tilt tuned or temperature tuned such that the phase offset satisfies $\phi_b = (n + 1/2)\pi$. Then $\cos\phi_b = 0$ implying that an equal number of partial periods of the sinusoidal filter are on each side of ω_b but having opposite sign. In the case where the filter width is not accurate enough to precisely satisfy $\hat{f}(\phi_b\kappa) = 0$ to achieve complete background suppression, this phase offset technique could also be applied to further suppress the background.

C. Standard PEM polarimetry

We look to incorporate a sinusoidal birefringent filter, as described in the Sec. III A, into the conventional dual PEM polarimeter of Sec. II A. This can be achieved by inserting a waveplate (delay ϕ) behind the second PEM as shown in Fig. 6. The initial PEM modulates the s_2 and s_3 components. The second PEM acts on all polarized Stokes components and modulates the phase of the sinusoidal filter to ensure signal at all Doppler shifts. The measured signal is

$$\begin{aligned} 2S(\omega) = {} & s_0(\omega) + s_1(\omega)\cos(\phi(\omega) + \delta_2) \\ & + s_2(\omega)\sin\delta_1 \sin(\phi(\omega) + \delta_2) \\ & - s_3(\omega)\cos\delta_1 \sin(\phi(\omega) + \delta_2). \end{aligned} \tag{19}$$

To maximise the signal with the new system, the final polarizer is now oriented at 0°, unlike in the conventional system, as the coherence technique requires signals with the delay, $\phi(\omega)$, for spectral discrimination of the orthogonally polarized components. Integrating over the Stark spectrum, the signal

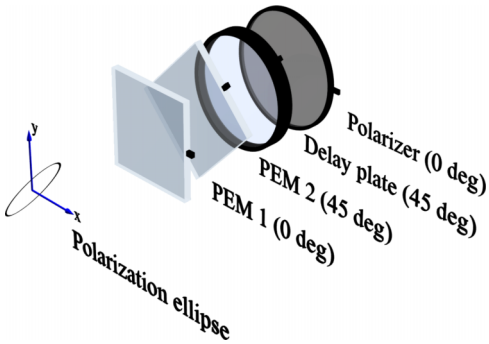

FIG. 6. Schematic model of the amplitude encoded, coherence based dual PEM arrangement for MSE polarimetry.

will be

$$2S = I_0 + \cos 2\theta_\sigma \left(\zeta_{\cos}\cos\delta_2 - \zeta_{\sin}\sin\delta_2\right) + \sin 2\theta_\sigma \sin\delta_1 \left(\zeta_{\cos}\sin\delta_2 - \zeta_{\sin}\cos\delta_2\right), \quad (20)$$

where

$$\zeta_{\cos} = \int_0^\infty I(\omega)p(\omega)f(\omega)\cos\phi(\omega)d\omega, \quad (21)$$

$$\zeta_{\sin} = \int_0^\infty I(\omega)p(\omega)f(\omega)\sin\phi(\omega)d\omega, \quad (22)$$

where $I(\omega)$ and $p(\omega)$ are defined in Eq. (3) and $f(\omega)$ is the transmission profile of the broad interference filter. This system is similar to the spatially modulated IMSE system described in Equation 6 of Ref. 17.

A consequence of including the delay is that the amplitude modulation of even harmonics is disrupted and the demodulation strategy must involve cross harmonics of ω_1 and ω_2. The amplitude at frequency $n\omega_1 + m\omega_2$ $(n \geq 0, m > 0)$ is

$$S_{|n\omega_1+m\omega_2|} = \begin{cases} \cos 2\theta_\sigma \zeta_{\cos} J_m(\phi_2) & n = 0,\ m \text{ even} \\ \cos 2\theta_\sigma \zeta_{\sin} J_m(\phi_2) & n = 0,\ m \text{ odd} \\ \sin 2\theta_\sigma \zeta_{\sin} J_n(\phi_1) J_m(\phi_2) & n \text{ odd},\ m \text{ even} \\ \sin 2\theta_\sigma \zeta_{\cos} J_n(\phi_1) J_m(\phi_2) & n \text{ and } m \text{ odd} \end{cases}. \quad (23)$$

The ζ terms are common to both $\sin 2\theta_\sigma$ and $\cos 2\theta_\sigma$ amplitudes in Eq. (23) and are maximised by selecting a delay plate of appropriate thickness. Therefore, apart from signal to noise effects, the polarimetric measurement is independent of the spectrum and filter profile. When spatially integrating all ray paths through the system, the effect of non-uniformities in the delay plate thickness will be limited to the ζ terms. Hence these non-uniformities will act to slightly reduce the amplitude of the harmonic signals but will not effect the polarization measurement.

There is potential for s_3 components produced from the Stark-Zeeman effect or non-ideal mirrors to contaminate the s_1 signals but this can be avoided by setting $\phi_1 = 2.4$ such that $J_0(\phi_1) = 0$.

D. Phase PEM polarimetry

An alternative system encodes the polarization angle in the phase of the first PEM as in Fig. 7 and is similar to the single PEM polarimeter in Sec. II B. The initial quarter-wave plate and PEM phase encode the polarization orientation. The following delay plate and PEM modulate the amplitude of the phase modulated polarization signal such that there is a strong signal for all Doppler shifts. The resultant signal is

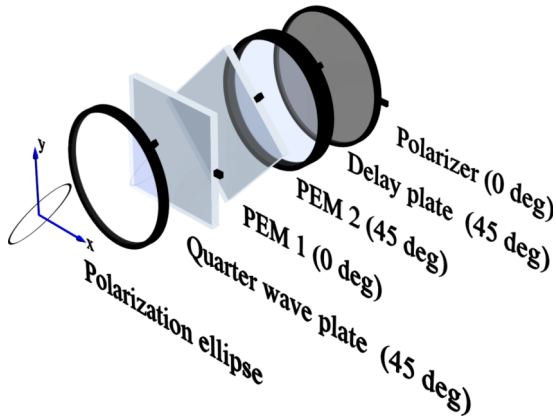

FIG. 7. Schematic model of the phase encoded, coherence based dual PEM arrangement for MSE polarimetry.

$$2S(\omega) = s_0(\omega) - s_1(\omega)\cos\delta_1 \sin(\phi(\omega) + \delta_2) + s_2(\omega)\sin\delta_1 \sin(\phi(\omega) + \delta_2) - s_3(\omega)\cos(\phi(\omega) + \delta_2). \quad (24)$$

The second PEM is used to modulate the sinusoidal filter phase; however, for a limited number of cases the phase ϕ_0 may already be close to an odd multiple of $\pi/2$ in which case the second PEM is not required ($\delta_2 = \phi_2 = 0$). For the MSE spectrum the signal is

$$2S = I_0 - \cos 2\theta_\sigma \cos\delta_1 \left(\zeta_{\sin}\cos\delta_2 + \zeta_{\cos}\sin\delta_2\right) + \sin 2\theta_\sigma \sin\delta_1 \left(\zeta_{\sin}\cos\delta_2 + \zeta_{\cos}\sin\delta_2\right). \quad (25)$$

This system is similar to the spatially modulated IMSE system described in Equation 7 of Ref. 17.

The amplitude at frequency $n\omega_1 + m\omega_2$ $(n, m > 0)$ is

$$S_{|n\omega_1+m\omega_2|} = \begin{cases} \cos 2\theta_\sigma \zeta_{\sin} J_n(\phi_1) J_m(\phi_2) & n \text{ and } m \text{ even} \\ \cos 2\theta_\sigma \zeta_{\cos} J_n(\phi_1) J_m(\phi_2) & n \text{ even},\ m \text{ odd} \\ \sin 2\theta_\sigma \zeta_{\sin} J_n(\phi_1) J_m(\phi_2) & n \text{ odd},\ m \text{ even} \\ \sin 2\theta_\sigma \zeta_{\cos} J_n(\phi_1) J_m(\phi_2) & n \text{ and } m \text{ odd} \end{cases}. \quad (26)$$

This phase encoded system is preferable to the standard PEM system as the s_3 component will be carried at $m\omega_2$ and will not contaminate the signal for s_1 and s_2. The s_1 signal power is dispersed across more carrier frequencies compared with the standard PEM system hence a fast digitiser is preferable to resolve as many frequencies as possible.

E. Separate polarimeter and interferometer

In Sections III C and III D the sinusoidal filter and polarization encoding are established within a single system. Knowledge of the spectrum is not required for these measurements as its effect is limited to the amplitudes expressed in Equations (21) and (22), which are common to the encoding

of both s_1 and s_2. A sequence of mirrors, required to shield the polarimeter from the harsh environment of ITER, is expected to significantly couple the components of the Stokes vector. In this situation it is necessary to calibrate the net Mueller matrix response of the mirrors and for the polarimeter to measure all components of the Stokes vector. However, when the polarimeter and interferometer are coupled, as in Equations (19) and (24), the s_0 component does not include the sinusoidal filter that is common to s_1, s_2 and s_3. Hence, if the mirror significantly transforms the Stokes vector the calibration would need to account for the spectrum of each of the Stokes components, which is generally not accurately known.

To apply a common sinusoidal filter to all of the Stokes components, it is necessary to separate the interferometer from the polarimeter.[22] Thus the standard dual PEM polarimeter of Sec. II A can remain unchanged with only modifications made to the filtering of the light at the detector end of the system as in Fig. 8. Light from the polarimeter is transmitted via optical fibres to the location of the detectors where the spectral filtering occurs. An initial interference filter transmits the desired full energy MSE component of the spectrum while the polarizer provides a common polarization for all components of the signal from the polarimeter. The sinusoidal spectral filter discussed in Sec. III A is established with a carefully selected delay or displacer plate. Finally, a Wollaston prism interferes the fast and slow rays providing two spatially separated signals for detection.

In Sec. III D the sinusoidal filter has been modulated to ensure periodic overlap with the spectrum as in Fig. 3. However, to avoid a third modulating element in the system, the waveplate must be temperature or tilt tuned to ensure the maximum or minimum of the sinusoidal filter remains approximately centered on the σ emission. Therefore this system is less naturally tolerant to changes in the neutral beam voltage; however, the waveplate could be further tilt tuned for operation at different voltages. The objective lens collimates the light such that there is a well defined correspondence between a ray's position in the optical fibre plane and its angle of intersection with the waveplate. The delay imposed between the fast and slow rays of a uniaxial crystal has a well defined angular dependence.[19] The delay of the crystal has an approximate linear angular dependence when its optic axis is cut at an angle to its surface and is known as a displacer waveplate. Hence, by carefully selecting the position of each optical fibre and the cut angle of the displacer's optic axis, each channel can acquire the delay required for maximum signal at its particular Doppler shift. Each optical fibre can be precisely positioned to correct for the nonlinearity of the Doppler shift with viewing angle.

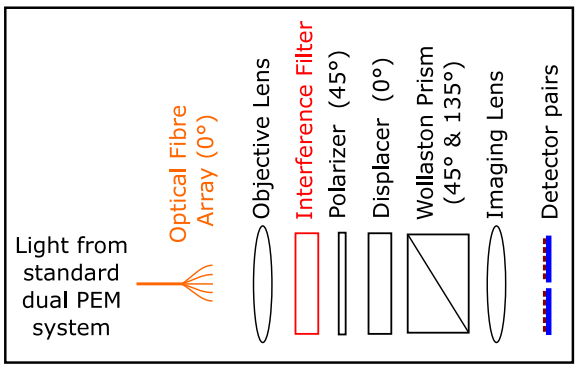

FIG. 8. Diagram of the interferometer component of the system. In a standard MSE polarimeter system each channel has an individual lens pair and narrowband interference filter. Here all channels can use the same lens pair and the narrowband interference filter is replaced by a broader interference filter along with a polarization interferometer. The polarization interferometer consists of a linear polarizer, displacer waveplate and Wollaston prism. The optical fibre array is aligned with the displacer waveplate such that each channel acquires an interferometric delay appropriate for its Doppler shift. Two detectors are needed for each channel due to the Wollaston prism producing two spatially separated images.

The signal measured using this interferometer along with the standard dual PEM polarimeter is

$$\begin{aligned} 8\sqrt{2}S_{\pm}(\omega) = \big(1 \pm \cos\phi(\omega,x)\big)\big(&\sqrt{2}s_0(\omega) + s_1(\omega)\cos\delta_2 \\ &+ s_2(\omega)(\cos\delta_1 + \sin\delta_1\sin\delta_2) \\ &+ s_3(\omega)(\sin\delta_1 - \cos\delta_1\sin\delta_2)\big), \end{aligned} \tag{27}$$

where the + sign is for the path through the Wollaston aligned with the initial polarizer and - sign for the anti-aligned path. The interferometer has simply multiplied Eq. (5) by $1 \pm \cos\phi(\omega,x)$. The x variable captures the dependence of the displacer's delay on the positioning of the optical fibre. Both signals from the Wollaston prism are needed, as individually the signals do not interfere the broadband background, due to the DC component from the interferometer. Taking the difference of S_+ and S_- signals provides a net signal that only contains the cosine filter and therefore suppresses the broadband background. An obvious requirement is for both signals to have the same detection efficiency and gain. With the MSE spectrum, the net signal would then be

$$\begin{aligned} 4\sqrt{2}(S_+ - S_-) = \sqrt{2}\int_0^\infty &s_0(\omega)\cos\phi(\omega)d\omega \\ &+ \cos 2\theta_\sigma\zeta_{\cos}\cos\delta_2 \\ &+ \sin 2\theta_\sigma\zeta_{\cos}(\cos\delta_1 + \sin\delta_1\sin\delta_2). \end{aligned} \tag{28}$$

Again the $\zeta_{\cos}$ term is common to both $\cos 2\theta_\sigma$ and $\sin 2\theta_\sigma$; hence, non-uniformities in the displacer thickness will not influence the inferred polarization orientation, apart from signal to noise effects. Another advantage is that the demodulation procedure is no different to the standard dual PEM system. s_0 and s_3 will also need to be determined from Eq. (27) to calibrate the effects of a non-ideal mirror.

After separating the interferometer from the polarimeter, all components of the Stokes vector are now carried with the same sinusoidal filter. Thus, provided that the mirrors are non-dispersive over the relatively small range of wavelengths and the polarization effects of the mirrors are known, it is possible to determine the sinusoidal filtered Stokes vector of the beam emission and the linear polarization orientation of the emission.

IV. EXPERIMENTAL VALIDATION

The reduction of the broadband polarized background signal was verified with a single PEM system (47 kHz) similar to that in Section III D but without the second PEM (Eq. (24) with $\delta_2 = 0$). A bright diffuse broadband light source was

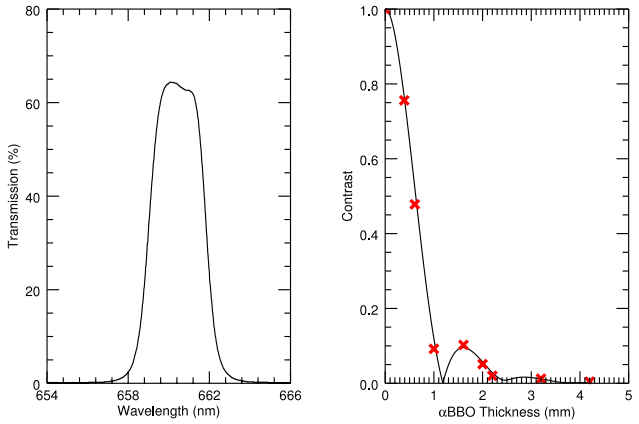

FIG. 9. Left: Filter transmission profile. Right: Magnitude of the filter transmission profile's Fourier transform (black line). Experimental data points for a selection of delay plate thicknesses—$|\hat{f}(\phi_b\kappa)|(\sin^2\phi_b + \cos^2\phi_b)$ (red crosses).

emitted from an integration sphere illuminated by a white halogen lamp. A film polarizer on the port of the integration sphere linearly polarized the light. The diffuse linearly polarized light passed through the single PEM polarimeter that had a minimum aperture of 30 mm. The polarimeter was followed by an interference filter with transmission profile as seen in Fig. 9. A 50 mm camera lens focused a collimated portion of the diffuse light on a photodetector with a digitizer sampling the signal at 400 kHz. The broadband polarization suppression was tested with a selection of delay plate thicknesses while keeping the interference filter fixed. To obtain a measurement independent of the sinusoidal filter phase ϕ_b, a second measurement was made with an achromatic waveplate aligned with each delay plate (Eq. (24) with $\delta_2 = \pi/2$). The amplitudes for both measurements are combined to determine the contrast of the linear polarization component of the signal for each delay plate. These experimental values are compared with the Fourier transform of the filter transmission profile as seen in Fig. 9.

Every collimated ray passing through a delay plate of uniform thickness will receive the same phase shift. Any small non-uniformities in the thickness of the delay plate and imperfect focusing of the lens will results in a range of phase shifts that reduce the effective signal strength, be it MSE spectrum signals or undesirable broadband background signals, but as seen in Fig. 9 any such effects were small.

When applying this technique to a fusion device such as ITER the crystal thickness would first be selected to maximise the polarization fraction and the filter profile subsequently specified to ensure background suppression for the chosen crystal thickness. For practicality the crystal thickness was varied for this validation as opposed to varying the filter width. If a 1.19 mm delay plate was required, then this particular filter would be tolerant to broadband polarized light.

V. ITER

The response of a coherence based PEM system has been modelled for an approximate ITER MSE spectrum as in Fig. 10. The spectrum assumes the bremsstrahlung

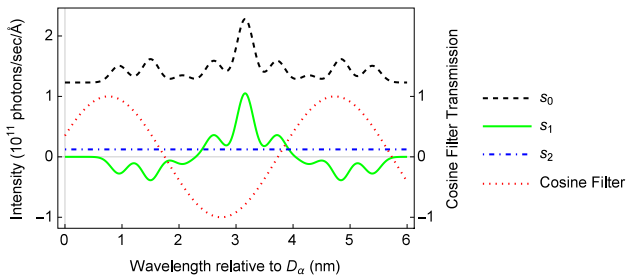

FIG. 10. Approximate polarization spectrum for ITER looking at the 100 keV diagnostic neutral beam with a magnetic field strength of B = 4.6 T and expected levels of bremsstrahlung background.[20] The system has been oriented such that $\theta_\sigma = 0°$ and the partially polarized background prescribed with $\theta_b = 45°$ and $p_b = 0.1$. The birefringent filter is αBBO with thickness $0.88\text{ mm} = 0.84L_0$.

background is partially polarized background with a 10% degree of polarization and orientated at the worst case scenario of 45° to the σ and π components. The delay plate is chosen with an optimal thickness of $0.84L_0$.

The effects of the filter width on the background suppression are illustrated in Fig. 11 for two idealised interference filter profiles. When the Lorentzian filter is wider than the MSE spectrum the background contamination of the polarization angle will reduce exponentially with increasing filter width. A real world filter function will incorporate features of both of these idealised filters, namely exponential reduction of the background contamination with filter width as well as some zero contrast crossings as in Fig. 9. With a wide enough filter or a precisely selected filter width the polarized broadband background contamination will vanish.

Other sources of light emission within the interference filter passband and their associated reflections require consideration as they have the potential to produce systematic errors in the measurement. Direct emission from wings of unshifted

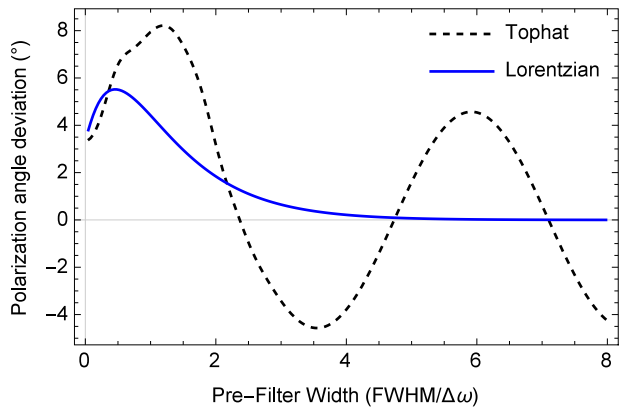

FIG. 11. Partially polarized broadband background contamination of the measured polarization angle from a coherence based PEM system. The filter is centred on the σ component such that $\phi_0 = \phi_b$. With tuning of ϕ_b the background can be minimised to any desirable level in one of the quadratures. For narrow interference filters the signal to background ratio initially decreases before the background begins to destructively interfere as the width is increased beyond $\Delta\omega$. For a top-hat filter, the contamination vanishes at the values given in Eq. (18). With a Lorentzian filter, the background contamination is suppressed exponentially with the filter FWHM. In this case a Lorentzian filter with FWHM = $4.75\Delta\omega = 7.9$ nm will limit the systematic error below 0.1°.

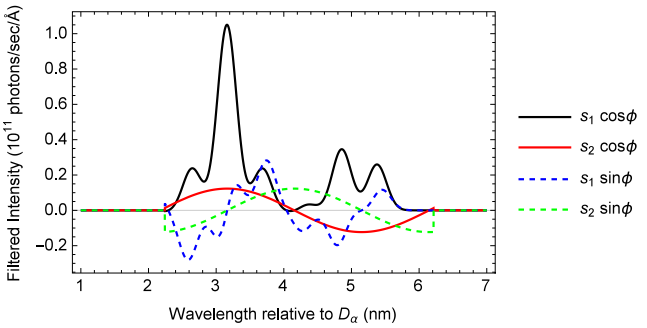

FIG. 12. Extreme example of the filtered ITER polarization spectra using a top-hat interference filter to target the broadband zero coherence crossing. Each spectrum is integrated to determine its measured signal amplitude. The width and offset of the top hat filter are chosen such that the broadband background signal of the cosine quadrature is negligible. Meanwhile the central σ peak is offset from the filter centre ($\phi_0 \approx \phi_b + 90°$) so that it maintains high throughput. Even though a π wing is almost completely blocked, the polarization throughput is $|\zeta| = 62\%$ of the total multiplet intensity i.e., larger than the <50% that would be achieved from only viewing the σ peak with a conventional PEM system.

D_α peaks and impurity emission will have a relatively small linear polarization fraction. Reflections of these features will have a greater polarization fraction but will have weaker intensity. Particularly impurity emission in the region of the MSE spectra is not expected to be significantly bright. The direct emission from half and third energy emissions from the neutral beam will have the same linear polarization orientation as the full energy component in the absence of a radial electric field, E_r. As a result leakage of these components may increase or decrease the signal strength but will not change the polarimetric results. In the case of significant E_r the polarization will deviate from the pure motional electric field and a correction will be required. Partially polarized reflection from the full energy emission is expected to be negligible compared to the direct emission. It is necessary for the viewing axis to only intersect a single neutral beam, as is expected on ITER, to avoid the second beams polarized emission from interfering with the signal from the desired beam.

If a steeper or narrower filter is required for a particular channel to further restrict any of the coherent partially polarized sources discussed above, then a separate individual filter could be tuned to target the phase offset $\phi_b = n\pi/2$ in addition to the filter width targeting the broadband coherence zero crossing. In this case one of the quadratures of ϕ_b would further minimise the background signal to any desired level even in the case when the filter width is not ideal. As an example a top-hat filter is applied over the diagnostic neutral beam signal of Fig. 10. These sine and cosine filtered Stokes spectra are illustrated in Fig. 12. In this example $|\hat{f}(\phi_b \kappa)| = 0$ and $\cos\phi_b = 0$ hence the background signal in the cosine quadrature is completely suppressed. Meanwhile $\cos\phi_0 \approx 1$ hence the polarized MSE signals are maximised in this quadrature.

VI. CONCLUSION

Coherence based MSE polarimeters have high throughput and intrinsically suppresses polarized broadband signals. The background signal can be reduced to any desirable level by selecting the interference filter transmission profile to match the period of the sinusoidal filter. With a single interference filter, multiple channels are accessible as well as operation over a range of beam energies. The system presented in Sec. III E is preferred due to the anticipated effects of non-ideal mirrors and does not require any changes to the polarimeter. The additional challenge for some channels of a coherence based system would be to select an interference filter that blocks other significant coherent sources of partially polarized light but is wide enough that the partially polarized broadband background destructively interferes completely. Conventional MSE system is advantageous when looking at signals with multiple beams or other polarized coherent contaminations as narrow filters can restrict undesired signals. However they cannot avoid partially polarized broadband backgrounds requiring subtraction strategies.

[1]F. M. Levinton, R. J. Fonck, G. M. Gammel, R. Kaita, H. W. Kugel, E. T. Powell, and D. W. Roberts, Phys. Rev. Lett. **63**, 2060 (1989).
[2]A. Boileau, M. von Hellerman, W. Mandl, H. P. Summers, H. Weisen, and A. Zinoviev, J. Phys. B: At., Mol. Opt. Phys. **22**, L145 (1989).
[3]R. Wolf, L.-G. Eriksson, M. V. Hellermann, R. König, W. Mandl, and F. Porcelli, Nucl. Fusion **33**, 1835 (1993).
[4]C. Petty, Y. Lin-Liu, T. Luce, M. Makowski, R. Prater, D. Schuster, H. S. John, and K. Wong, Nucl. Fusion **41**, 551 (2001).
[5]C. Petty, R. Prater, J. Lohr, T. Luce, W. Fox, R. Harvey, J. Kinsey, L. Lao, and M. Makowski, Nucl. Fusion **42**, 1366 (2002).
[6]C. A. Michael, A. Thorman, J. Chung, Y. S. Bae, J. H. Jeong, J. Decker, and J. Howard, "Electron Cyclotron current drive studies on KSTAR using imaging MSE," in presented at the 42nd EPS Conference on Plasma Physics, Lisbon, Portugal, 22-26 June 2015, available at http://ocs.ciemat.es/EPS2015PAP/pdf/O4.126.pdf.
[7]H. A. Bethe and E. E. Salpeter, *Quantum Mechanics of One- and Two-Electron Atoms* (Plenum, New York, NY, 1977).
[8]B. Rice, K. Burrell, and L. Lao, Nucl. Fusion **37**, 517 (1997).
[9]R. Mumgaard and S. Scott, "Engineering the Alcator C-Mod MSE diagnostic: Solutions to reactor-relevant diagnostic challenges," PSFC Report No. PSFC/JA-15-28, June 2015, available at http://library.psfc.mit.edu/catalog/reports/2010/15ja/15ja028/15ja028_abs.html.
[10]T. Fujita, H. Kuko, T. Sugie, N. Isei, and K. Ushigusa, Fusion Eng. Des. **34–35**, 289 (1997).
[11]P. Lotte, M. H. Aumeunier, P. Devynck, C. Fenzi, V. Martin, and J. M. Travère, Rev. Sci. Instrum. **81**, 10E120 (2010).
[12]S. Kajita, M. De Bock, M. von Hellermann, A. Kukushkin, and R. Barnsley, Plasma Phys. Controlled Fusion **75**, 045009 (2015).
[13]D. Voslamber, Rev. Sci. Instrum. **66**, 2892 (1995).
[14]D. Wróblewski, K. H. Burrell, L. L. Lao, P. Politzer, and W. P. West, Rev. Sci. Instrum. **61**, 3552 (1990).
[15]J. Kemp, G. Henson, C. Steiner, and E. Powell, Nature **326**, 270 (1987).
[16]J. Howard, Plasma Phys. Controlled Fusion **50**, 125003 (2008).
[17]J. Howard and J. Chung, Rev. Sci. Instrum. **83**, 10D510 (2012).
[18]O. P. Ford, J. Howard, and R. C. Wolf, Rev. Sci. Instrum. **86**, 093504 (2015).
[19]F. E. Veiras, L. I. Perez, and M. T. Garea, Appl. Opt. **49**, 2769 (2010).
[20]E. L. Foley, F. M. Levinton, H. Y. Yuh, and L. E. Zakharov, Rev. Sci. Instrum. **79**, 10F521 (2008).
[21]J. Howard, C. Michael, H. Chen, R. Lester, A. Thorman, and J. Chung, J. Instrum. **10**, P09023 (2015).
[22]J. Howard, Plasma Phys. Controlled Fusion **41**, 271 (1999).